

RESEARCH ARTICLE

Coordinated control for unbalanced operation of stand-alone doubly fed induction generator

Xing Li, Yao Sun, Mei Su and Hui Wang

School of Information Science and Engineering, Central South University, Changsha 410083, China

ABSTRACT

This paper proposes a coordinated control scheme of a stand-alone doubly fed induction generator (DFIG)-based wind energy conversion system to improve the operation performance under unbalanced load conditions. To provide excellent voltage profile for load, a direct stator flux control scheme based on auto-disturbance rejection control (ADRC) is applied, and less current sensors are required. Due to the virtues of ADRC, the controller has good disturbance rejection capability and is robust to parameter variation. In the case of unbalanced loads, the electromagnetic torque pulsations at double synchronous frequency will exist. To eliminate the undesired effect, the stator-side converter (SSC) is used to provide the negative sequence current components for the unbalanced load. Usually, proportional integral controllers in a synchronous reference frame are used to control SSC. To simplify the algorithm, an improved proportional resonant (PR) control is proposed and used in the current loop without involving positive and negative sequence decomposition. The improved PR provides more degree of freedom which could be used to improve the performance. The effectiveness of the proposed control scheme has been validated by the simulation and experimental results. Copyright © 2012 John Wiley & Sons, Ltd.

KEYWORDS

auto-disturbance rejection control (ADRC); doubly fed induction generator (DFIG); proportional resonant (PR) controller; stand-alone wind-power generation; unbalance

Correspondence

M. Su, School of Information Science and Engineering, Central South University, Changsha 410083, China.

E-mail: xingliaaa@gmail.com

Received 4 November 2011; Revised 18 September 2012; Accepted 3 November 2012

1. INTRODUCTION

The doubly fed induction generator (DFIG) is widely used for variable speed generation and is one of the most important generators for wind energy conversion system,^{1,2} in either grid-connected or stand-alone operation. Usually, three-phase AC/DC/AC converter is employed as the power electronics interface, which consists of rotor-side and stator-side pulse-width modulation (PWM) converters connected back-to-back. The main advantage for the wind power system based on DFIG is that the power electronics converter is sized only for a part of the generator rated power, proportional to the operational speed range.

Nowadays, the grid-connected wind power systems based on DFIG have been studied widely,^{1–7} whereas the stand-alone systems^{8–10} are rarely raised as a problem for discussion. However, in rural communities and remote areas, the extension of grid is not economically viable, and the power quality cannot fulfill the local power requirements. Therefore, with the backup support from other generators, the stand-alone DFIG system would be more suitable to supply power for the isolated loads, or supplement the real power demand of the grid by integrating power from resources located at different sites.

In the beginning, the self-excited power generation system based on squirrel cage induction machine offered several advantages over conventional synchronous generators as a source of stand-alone power supply. These are lower cost, brushless rotor, ease of maintenance, relatively high reliability and so on.¹¹ However, the disadvantage is that the voltage and frequency are difficult to control, and it should be equipped with reactive power compensation devices. Therefore, they are just sporadically applied in new installations of large power. Although this wind power system can be controlled more simply with the development of power electronics technology, the total cost of power generation increases greatly. In addition, a stand-alone wind energy conversion system based on DFIG was reported in 1996,⁸ where it was proposed to use vector-control scheme for generating electricity, and it proved to be correct by experiments. The vector-control method described in the work of Cardenas

*et al.*⁹ replaced the mechanical encoder by an estimator based on model reference adaptive system (MRAS) observer. Besides, a simple direct voltage control method of stand-alone operation was presented in the work of Iwanski and Koczara,¹⁰ which required no rotor position encoder.

In grid-connected application, many research efforts have devoted to improve the performance of DFIG-based wind power system under unbalanced grid voltage conditions. Because the negative sequence currents can produce torque and power pulsations at double synchronous frequency and localized overheat in the stator and rotor, this may result in acoustic noise and fatigue on the mechanical components and reduce the system life cycle. Thus, to protect the machine, control systems for the operation of DFIG under unbalanced grid have been reported in the works of Xu¹² and Hu and He,¹³ where they focused on how to effectively control the negative sequence currents of rotor-side converter (RSC) and/or stator-side converter (SSC) to eliminate the torque pulsations. Usually, dual-current proportional integral (PI) controllers were employed by decomposing the positive and negative sequence components.¹² In the work of Hu and He,¹³ enhanced control and operation by using proportional resonant (PR) controllers were implemented without involving the sequential decomposition.

However, in the case of unbalanced or nonlinear loads under stand-alone operation, DFIG-based wind power systems also suffered from negative sequence or high order harmonic contents. Therefore, control methods for compensating the effects of unbalanced load were presented in the works of Phan *et al.*, Jain and Ranganathan and Pena *et al.*,^{14–16} and the work of Jain and Ranganathan¹⁵ explored the potential of SSC functioned as an active power filter, which made DFIG operation free from the impact of undesirable currents, but increased the control complexity.

In this paper, a coordinated control strategy for the RSC and SSC of a stand-alone wind energy conversion system based on DFIG is proposed under unbalanced load condition. As for the RSC, auto-disturbance rejection control (ADRC)¹⁷ is used to achieve the voltage control scheme indirectly. Then, from the control point of view, this paper gives a thorough analysis for its feasibility and factors that affect the control performance. In order to suppress the impacts of unbalanced loads, the SSC takes the responsibility for providing negative sequence currents for the loads, which makes DFIG operation free from negative sequence components. Besides, a current control method based on improved PR controllers in the stationary reference frame is presented, which makes the control design quite simple. Simulation and experimental results on a stand-alone wind power system based on DFIG verify the correctness and effectiveness of the coordinated control scheme.

2. SYSTEM MODELING

The overall configuration of the stand-alone wind power system based on DFIG is depicted in Figure 1, which consists of the wind turbine, DFIG, AC/DC/AC power electronics converters, filtering capacitors and load. In contrast to the classical grid-connected system, the load does not mean the grid but the passive load. As for the converters, the RSC is used to ensure that DFIG can obtain the output voltage with certain amplitude and frequency, and the SSC provides appropriate common DC-link voltage for the power converters. Usually, to achieve the desirable output voltage, filtering capacitors are connected to the stator, which is a part of the output low-pass filter together with the equivalent leakage inductance in DFIG.

According to Figure 1, the per-phase equivalent circuit can be drawn in the stationary reference frame, as shown in Figure 2. Then, a detailed space-vector model of the stand-alone wind power system based on DFIG can be described as follows:

$$\vec{u}_s = R_s \vec{i}_s + \frac{d\vec{\psi}_s}{dt} \quad (1)$$

$$\vec{u}_r = R_r \vec{i}_r + \frac{d\vec{\psi}_r}{dt} - j\omega_r \vec{\psi}_r \quad (2)$$

$$\vec{\psi}_s = L_s \vec{i}_s + L_m \vec{i}_r \quad (3)$$

$$\vec{\psi}_r = L_r \vec{i}_r + L_m \vec{i}_s \quad (4)$$

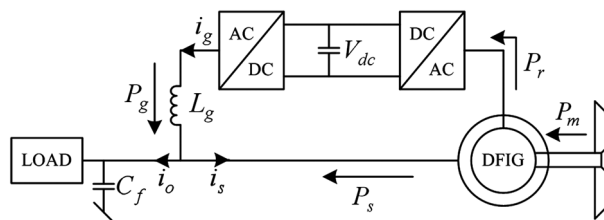


Figure 1. Configuration of the stand-alone system based on DFIG.

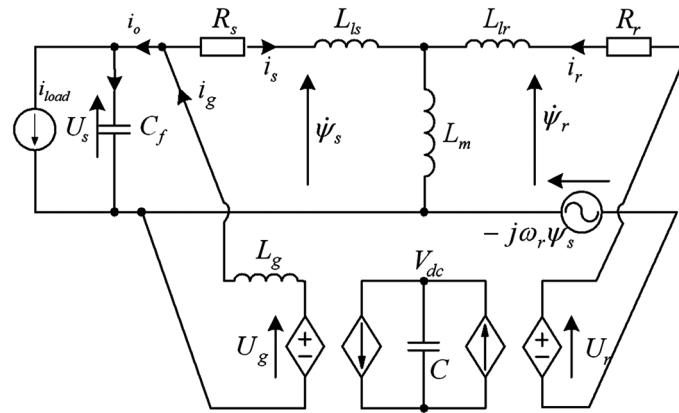


Figure 2. Per-phase equivalent circuit of the stand-alone system based on DFIG.

$$C_f \frac{d\vec{u}_s}{dt} = \vec{i}_o - \vec{i}_{\text{load}} = \vec{i}_g - \vec{i}_s - \vec{i}_{\text{load}} \quad (5)$$

$$L_g \frac{d\vec{i}_g}{dt} = \vec{u}_g - \vec{u}_s - R_g \vec{i}_g \quad (6)$$

$$V_{\text{dc}} C \frac{dV_{\text{dc}}}{dt} = P_{\text{g}} - P_{\text{r}} = \frac{3}{2} \left(\vec{u}_{\text{s}} \bullet \vec{i}_{\text{g}} - \vec{u}_{\text{r}} \bullet \vec{i}_{\text{r}} \right) \quad (7)$$

where (1)–(4) represent the dynamics of DFIG, (5) represents the characteristic equation of filtering capacitors, (6)–(7) indicate the mathematic models of the dual-PWM converter and the operator ‘ \cdot ’ in (7) stand for inner product. \vec{u}_s , $\vec{\psi}$ and \vec{i} are the voltage, flux and current vectors, respectively. R represents the resistance of each winding; subscripts s, r and g denote the quantities in the stator, rotor and SSC, respectively. \vec{i}_{load} is the load current vector, and \vec{i}_g the current vector flowing through filtering inductor L_g of the SSC. L_s and L_r are the self-inductance of the stator and rotor windings, respectively. L_m is the mutual inductance between the stator and rotor. ω_s and ω_r are the system and rotor angular frequencies, respectively. V_{dc} is the DC-link voltage.

3. COORDINATED CONTROL OF RSC AND SSC

Nowadays, the grid-connected operation based on DFIG has been well developed. Usually, the real and reactive powers are considered as control targets, which can be transformed into controlling the real and reactive components of stator current, since the stator voltages are determined by the grid.

However, in the stand-alone system, the magnitude and frequency of the stator voltage should be controlled simultaneously to guarantee the normal operation of load. Moreover, the control strategies will vary with the nature of load. For linear and balanced one, the system variables are sinusoidal and easy to control; but if the unbalanced loads occur, a more complicated control method, which is the focus of this paper, should be used to protect the DFIG system from negative sequence components.

3.1. Power flow graph

The power flow graph of the stand-alone system based on DFIG is shown in Figure 3. According to principle of conservation of power, the real powers in the system can be expressed as

$$P_0 = P_s + P_g \quad (8)$$

$$P_r = P_g + P_c \quad (9)$$

$$P_s = P_m - P_{\text{loss}} - P_r \quad (10)$$

where P_o , P_g , P_s , P_r , P_c and P_m are the real powers of the load, SSC, stator, rotor, common DC-link capacitor and mechanical part, respectively; P_{loss} represents power loss including copper and core loss.

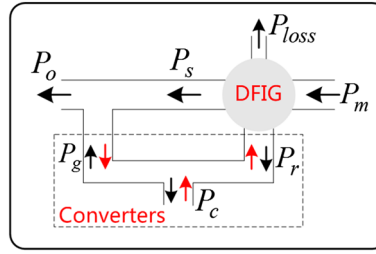


Figure 3. Power flow graph of the stand-alone system based on DFIG.

Because of the unbalanced load, the load power can be expressed as $P_o = \bar{P}_o + \tilde{P}_o$, where \bar{P}_o and \tilde{P}_o are the DC and AC components, respectively. Therefore, the stand-alone system may operate in the following two modes depending on different control purposes.

In the first mode, $P_g = \bar{P}_g$ namely, the SSC is under balanced operation. According to (8)–(10) and neglecting the power loss P_{loss} , we have $\tilde{P}_s = \tilde{P}_o = \tilde{P}_m - \tilde{P}_r$ and $\tilde{P}_r = \tilde{P}_c$. Besides, the electromagnetic torque that can be expressed as $T_e = 1.5p(\vec{\psi}_s \times \vec{i}_s)$ contains second harmonic content, because of the negative sequence component in \vec{i}_s . Therefore, this mode will cause torque pulsations and localized overheat in the machine.

In the second mode, $\tilde{P}_g = \tilde{P}_o$ namely, the AC component of the load power is provided by the SSC. According to (8)–(10) and neglecting P_{loss} , we have $\tilde{P}_s = 0$ and $\tilde{P}_o = \tilde{P}_g = -\tilde{P}_c$. Thus, the variables in the machine do not contain negative sequence components, and the AC power just run back and forth between loads and DC-link capacitor. As a result, the unexpected effect of energy distribution in other parts of the system can be avoided; this mode is adopted in this paper. However, it is worth noting that the AC power of the DC-link capacitor may increase, that is to say, the DC-link voltage would oscillate more seriously.

3.2. Stator flux control for the rotor-side converter

In this section, the stator flux is considered as the intuitive control target instead of the stator voltage. However, the desired stator voltage will be obtained consequently.

In order to ensure the normal operation of load, the stator voltage performance should be guaranteed first, namely, let

$$\lim_{t \rightarrow \infty} \vec{u}_s = \vec{u}_s^* \quad (11)$$

Assume that the stator flux has been in the steady state through appropriate control and the stator flux $\vec{\psi}_s$ equals to its reference $\vec{\psi}_s^*$, then (1) can be rewritten as

$$\vec{i}_s = \frac{\vec{u}_s - j\omega_s \vec{\psi}_s^*}{R_s} \quad (12)$$

If the stator resistance is small enough, even though the rotor currents are unbalanced, the stator voltages can also be considered symmetrical approximately.

Substituting (12) into (5) yields

$$C_f \frac{d\vec{u}_s}{dt} = -\frac{\vec{u}_s}{R_s} + \frac{j\omega_s \vec{\psi}_s^*}{R_s} + \vec{i}_g - \vec{i}_{load} \quad (13)$$

where the last three items on the right can be regarded as a bounded disturbance in a unified way. Obviously, (13) is stable. Therefore, when the stator flux reaches its steady state, the stator voltage will converge to \vec{u}_s^* automatically. In addition, the filtering capacitors C_f are mainly used to mitigate the output voltage harmonics and to provide appropriate reactive power for load. According to (13), the larger the capacitance is, the better the filtering performance is; however, it might slow down the system dynamic response as well. Hence, the filtering capacitor should be chosen by considering the trade-off between filtering performance, reactive power requirement and dynamic response.

According to (3) and (4), the stator current and rotor flux can be expressed using the rotor current and stator flux as

$$\vec{i}_s = \frac{\vec{\psi}_s - L_m \vec{i}_r}{L_s} \quad (14)$$

$$\vec{\psi}_r = \delta L_r \vec{i}_r + \frac{L_m}{L_s} \vec{\psi}_s \quad (15)$$

where $\delta = 1 - \frac{L_m^2}{L_s L_r}$.

Substituting (14) into (1) leads to

$$\frac{d\vec{\psi}_s}{dt} = -\frac{R_s}{L_s} \vec{\psi}_s + \frac{R_s L_m}{L_s} \vec{i}_r + \vec{u}_s \quad (16)$$

Then, combining (2), (15) and (16) yields

$$\delta L_r \frac{d\vec{i}_r}{dt} = \left(-R_r - \frac{R_s L_m^2}{L_s^2} + j\omega_r \delta L_r \right) \vec{i}_r + \frac{L_m}{L_s} \left(\frac{R_s}{L_s} + j\omega_r \right) \vec{\psi}_s + \vec{u}_r - \frac{L_m}{L_s} \vec{u}_s \quad (17)$$

Decompose (16) and (17) in the synchronous (D - Q) reference frame as

$$\frac{d\psi_{sd}}{dt} = -\frac{R_s}{L_s} \psi_{sd} + \omega_s \psi_{sq} + \frac{R_s L_m}{L_s} i_{rd} + u_{sd} \quad (18)$$

$$\frac{d\psi_{sq}}{dt} = -\frac{R_s}{L_s} \psi_{sq} - \omega_s \psi_{sd} + \frac{R_s L_m}{L_s} i_{rq} + u_{sq} \quad (19)$$

$$\frac{di_{rd}}{dt} = \left(-\frac{R_r}{\delta L_r} - \frac{R_s L_m^2}{L_s^2 \delta L_r} \right) i_{rd} + (\omega_s - \omega_r) i_{rq} + \frac{L_m R_s}{L_s^2 \delta L_r} \psi_{sd} - \frac{L_m \omega_r}{L_s \delta L_r} \psi_{sq} + \frac{1}{\delta L_r} u_{rd} - \frac{L_m}{L_s \delta L_r} u_{sd} \quad (20)$$

$$\frac{di_{rq}}{dt} = \left(-\frac{R_r}{\delta L_r} - \frac{R_s L_m^2}{L_s^2 \delta L_r} \right) i_{rq} - (\omega_s - \omega_r) i_{rd} + \frac{L_m R_s}{L_s^2 \delta L_r} \psi_{sq} + \frac{L_m \omega_r}{L_s \delta L_r} \psi_{sd} + \frac{1}{\delta L_r} u_{rq} - \frac{L_m}{L_s \delta L_r} u_{sq} \quad (21)$$

where (18) and (20), (19) and (21) are the D and Q axes electric dynamic equations of DFIG, respectively.

In this section, ADRC is used to control the stator flux instead of the conventional dual-loop PI control. As in the work of Han,¹⁷ ADRC consists of a tracking differentiator (TD), a state feedback combination (SFC) of proportional, integral and differential errors and an extended state observer (ESO) for the total disturbance estimation and rejection. The goodness of ADRC over PI control is that it can achieve the feedback linearization of dynamic system and improve the capability to inhibit the error signal by nonlinear feed-forward compensation.

Since the control principles of ADRC in D and Q axes are similar, D -axis has been taken as an example to give design steps in detail. Because the electric dynamics of DFIG can be regarded as a second-order system, the following second-order state space representation is considered.

$$\begin{cases} y = x_1 \\ \dot{x}_1 = x_2 \\ \dot{x}_2 = f(x_1, x_2, \varpi(t), t) + bu \end{cases} \quad (22)$$

where x_1 is the system state, x_2 is the first time derivative of x_1 , y is the output, u is the control input, $\varpi(t)$ is the external disturbance and b is the high frequency gain. $f(x_1, x_2, \varpi(t), t)$ represents both the internal dynamics and the external disturbance of the system. If $f(x_1, x_2, \varpi(t), t)$ can be observed by the ESO in real time, they will be actively compensated by ADRC without the need to know its explicit mathematical expression.

First, the D -axis system equations (18) and (20) should be transformed into the form as (22), namely,

$$\begin{cases} y = x_1 = \psi_{sd} \\ \dot{x}_1 = \dot{\psi}_{sd} = x_2 \\ \dot{x}_2 = \underbrace{(Mx_1 + Nx_2 + \omega_s \dot{\psi}_{sq} + \dot{\psi}_{sd} + J)}_{f(x_1, x_2, \varpi(t), t)} + \underbrace{(R_s L_m / \delta L_r L_s) u_{rd}}_{bu} \end{cases} \quad (23)$$

where

$$\begin{aligned} M &= -\frac{R_s R_r}{\delta L_r L_s}; N = -\frac{R_s}{L_s} - \frac{R_r}{\delta L_r} - \frac{R_s L_m^2}{\delta L_r L_s^2} \\ J &= \frac{R_r}{\delta L_r} (\omega_s \psi_{sq} + u_{sd}) + \frac{R_s L_m (\omega_s - \omega_r)}{L_s} \left(i_{rq} + \frac{L_m}{\delta L_r L_s} \psi_{sq} \right) \end{aligned}$$

Then, the corresponding control block diagram of the second-order ADRC is shown in Figure 4, where the reference v and the output y are both considered as the inputs of ADRC and u is its output. Assume that the expected D -axis stator flux is ψ_{sd}^* , which is equivalent to the reference v in Figure 4. Usually, a feasible second-order TD can be designed as

$$\begin{aligned} \dot{v}_1 &= v_2 \\ \dot{v}_2 &= -r \cdot \text{sgn} \left(v_1 - v(t) + \frac{v_2 |v_2|}{2r} \right) \end{aligned} \quad (24)$$

where r is a positive parameter. For simplicity, let $v_1 = \psi_{sd}^*$, and $v_2 = 0$. Then, the SFC of proportional and differential errors can be constructed as follows:

$$u_0 = k_1 e_1 + k_2 e_2 \quad (25)$$

where k_1 and k_2 are the control gains, usually, they could be selected as $k_1 = \omega_c^2$ and $k_2 = 2\eta\omega_c$, where ω_c is the controller bandwidth, and η is the damping ratio. From (23), the disturbance $f(x_1, x_2, \varpi(t), t)$ is viewed as an extended state variable $x_3 = f(x_1, x_2, \varpi(t), t)$. Using z_1 , z_2 and z_3 to estimate x_1 , x_2 and x_3 , respectively, the ESO can be designed as

$$\begin{cases} e = z_1 - y \\ \dot{z}_1 = z_2 - \beta_1 e \\ \dot{z}_2 = z_3 - \beta_2 \text{fal}(e, \alpha_1, \delta) + bu \\ \dot{z}_3 = -\beta_3 \text{fal}(e, \alpha_2, \delta) \end{cases} \quad (26)$$

where β_1 , β_2 and β_3 are observer gains, and $\text{fal}(e, \alpha, \delta)$ is a nonlinear function described by

$$\begin{cases} \frac{e}{\delta^{1-\alpha}}, & |x| \leq \delta \\ |e|^\alpha \text{sgn}(e), & |x| \geq \delta \end{cases}$$

where both α and δ are positive values. Once the extended observer (26) is well tuned, its output will track the states and disturbance with very small error, respectively. Then, ADRC can compensate the disturbance $f(x_1, x_2, \varpi(t), t)$ in real time in the feed-forward manner. At last, the controller is designed as

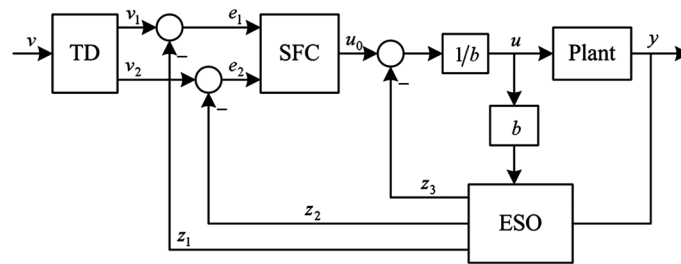


Figure 4. Control structure of the second-order ADRC.

$$u = \frac{u_0 - z_3}{b} \quad (27)$$

So, the D -axis stator flux control with ADRC is completed by the appropriate adjustment of various parameters. The design of Q -axis controllers can also use the same method earlier, which is not discussed here in detail. Thus, the overall schematic diagram of the proposed stator flux control is shown in Figure 5.

Neglecting the stator resistance and taking (1) into account, the steady-state equation is

$$\bar{u}_s = j\omega_s \bar{\psi}_s \quad (28)$$

Then, the expected stator flux ψ_{sd}^* and ψ_{sq}^* are

$$\psi_{sd}^* = \left| \frac{\bar{u}_s}{\omega_s} \right| \quad \psi_{sq}^* = 0 \quad (29)$$

As can be seen in Figure 5, to obtain the expected angular frequency $\omega_s^* = 314 \text{ rad s}^{-1}$, the angular position of the stator flux is set as $\theta_s = \int \omega_s^* dt$. The feedback ψ_{sd} and ψ_{sq} are calculated and transformed from

$$\bar{\psi}_s = \int (\bar{u}_s - R_s \bar{i}_s) dt \quad (30)$$

Moreover, since the stator resistance is ignored, the control accuracy of output voltage has decreased inevitably. Therefore, a simple PI controller is used to correct the expected D -axis stator flux, i.e.

$$\psi_{sd}^* = \left| \frac{\bar{u}_s^*}{\omega_s} \right| + k_{pu} \cdot (|\bar{u}_s^*| - |\bar{u}_s|) + k_{iu} \cdot \int (|\bar{u}_s^*| - |\bar{u}_s|) dt \quad (31)$$

It is worth noting that the impact of stator resistance can be neglected only in the case of small stator current. Once the output power increases, the stator voltage distortion caused by unbalanced stator current will be more severe. In that case, the basic output voltage performance cannot be guaranteed, which is not allowed for the stand-alone operation. Therefore, for the unbalanced load condition, the control of RSC should be complemented by the SSC.

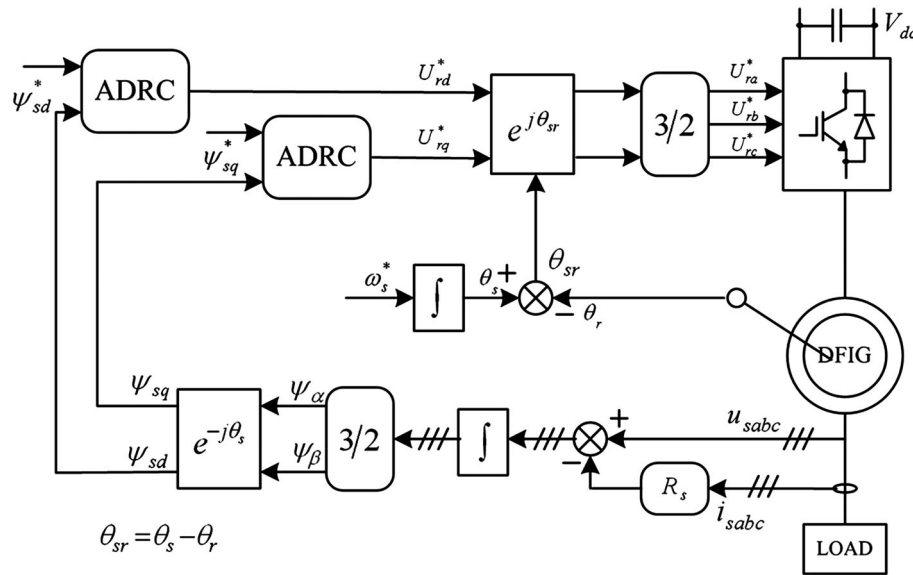


Figure 5. Schematic diagram of the stator flux control based on ADRC.

3.3. Control for the stator-side converter

Under the unbalanced load condition, if the negative sequence components of the load currents are provided by the SSC, then torque pulsations and localized overheat in the machine will be eliminated. In that case, \vec{u}_s and \vec{i}_g can be expressed as

$$\vec{u}_s = \left| \vec{u}_s \right| e^{j\omega_s t} \quad (32)$$

$$\vec{i}_g = i_g^+ e^{j\omega_s t} + i_g^- e^{-j\omega_s t} \quad (33)$$

where i_g^+ and i_g^- are the positive and negative sequence components of \vec{i}_g in the stationary reference frame, respectively. Substituting (32) and (33) into (7) yields

$$V_{dc} C \frac{dV_{dc}}{dt} = P_g - P_r = \frac{3}{2} \left[\left| \vec{u}_s \right| i_{gd}^+ + \left| \vec{u}_s \right| i_{gd}^- \cos(2\omega_s t) + \left| \vec{u}_s \right| i_{gq}^- \sin(2\omega_s t) - \vec{u}_r \bullet \vec{i}_r \right] \quad (34)$$

Then, decompose (34) into the following two parts:

$$\bar{V}_{dc} C \frac{d\bar{V}_{dc}}{dt} = \bar{P}_g - \bar{P}_r = \frac{3}{2} \left(\left| \vec{u}_s \right| i_{gd}^+ - \vec{u}_r \bullet \vec{i}_r \right) \quad (35)$$

$$V_{dc} C \frac{d\tilde{V}_{dc}}{dt} + \tilde{V}_{dc} C \frac{d\bar{V}_{dc}}{dt} = \tilde{P}_g = \frac{3}{2} \left[\left| \vec{u}_s \right| i_{gd}^- \cos(2\omega_s t) + \left| \vec{u}_s \right| i_{gq}^- \sin(2\omega_s t) \right] \quad (36)$$

where (35) represents the DC part and (36) is the AC part. Once (35) reaches steady state, \tilde{V}_{dc} can be obtained by integrating (36), which contains second harmonic content actually. However, this paper only considers \bar{V}_{dc} as the need for control.

According to (35), the DC part of the DC-link voltage can be controlled by regulating i_{gd}^+ properly. \bar{V}_{dc} could be extracted through a low-pass filter or notch filter. For a fast dynamic response, a notch filter is used here.

Generally, the dual-loop PI controllers are used in the positive and negative sequence synchronous reference frames, respectively. However, the sequential separation is indispensable, which makes the control design more complicated. There are two methods usually used for the separation of the positive and negative sequence components. One is to use the transformation of coordinates (ABC to $D-Q$) and notch filter. The other is the 'signal delay cancellation' method.¹³ However, whatever it takes, the time delay and certain errors in amplitude and phase would be introduced inevitably, and then, the transient performance would be degraded. For these reasons, PR controllers are used to regulate the current loop without involving the sequential decomposition, which can reduce the computational effort and simplify the control algorithm.

According to the analysis earlier, the schematic diagram of the SSC control is shown in Figure 6. In the digital implement of the PR controller, the impulse invariant discretization method is used to obtain the infinite gain at the desired frequency.^{18,19} As PR controllers are capable of tracking sinusoidal signal precisely, first, decompose (6) in the stationary reference frame into

$$L_g \frac{di_{gz\beta}}{dt} = u_{gz\beta} - u_{sz\beta} - R_g i_{gz\beta} \quad (37)$$

Then, an improved PR control in Laplace domain can be designed from (37) as follows:

$$u_{gz\beta}(s) = u_{sz\beta}(s) + (R_g - k) i_{gz\beta}(s) + F_{PR}(s) \left[i_{gz\beta}^*(s) - i_{gz\beta}(s) \right] \quad (38)$$

where the first term on the right of (38) is the feed-forward item and the second one denotes the local feedback that can be regarded as a degree of control freedom. Besides, $F_{PR}(s) = k_p + k_r s / (s^2 + \omega_s^2)$ represents the PR controller, and k_p and k_r are the proportional and resonant parameters, respectively.

The block diagram of the proposed PR control for the SSC is shown in Figure 7. Considering the time delay caused by sampling and calculation, the open-loop transfer function of the PR control can be obtained as follows:

$$L(s) = \frac{k_p}{k} \frac{1}{\tau s + 1} \left(1 + \frac{k_r}{k_p} \frac{s}{s^2 + \omega_s^2} \right) e^{-T_D s} \quad (39)$$

where $\tau = L_g/k$ and T_D denotes the control delay time. When the cross-over frequency $\omega_c \gg \omega_s$, $L(s)$ could be approximated as

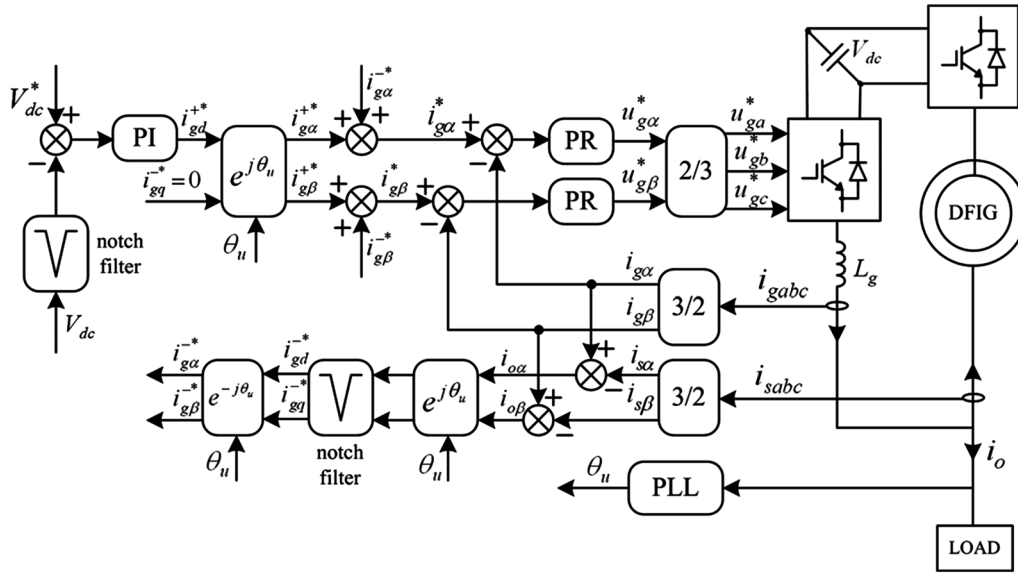


Figure 6. Schematic diagram of the SSC control based on PR.

$$L(s) = \frac{k_r}{k} \frac{(k_p/k_r s + 1)}{s(\tau s + 1)} e^{-T_D s} \quad (40)$$

If $k_p/k_r = \tau$, then

$$\angle L(j\omega_c) = -\frac{\pi}{2} - \omega_c T_D = -\pi + \theta_m \quad (41)$$

$$\omega_c = \left(\frac{\pi}{2} - \theta_m\right)/T_D \quad (42)$$

$$|L(j\omega_c)| = \frac{k_r}{\omega_c k} = 1 \quad (43)$$

where θ_m is the required phase margin for system stability. If τ has been determined, it is easy to complete the whole design of the PR controllers. The larger τ is, the faster the response is; the smaller τ is, the less the steady-state error at the resonant frequency is and the less sensitive to the frequency variation is. The Bode diagram shown in Figure 8 could verify the correctness of the proposed design method.

In order to eliminate the negative sequence components in the stator currents, the negative sequence current reference of the SSC should be

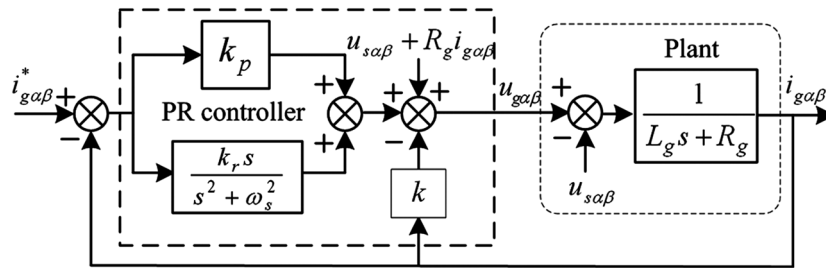


Figure 7. Diagram of the PR controller for the stator-side converter.

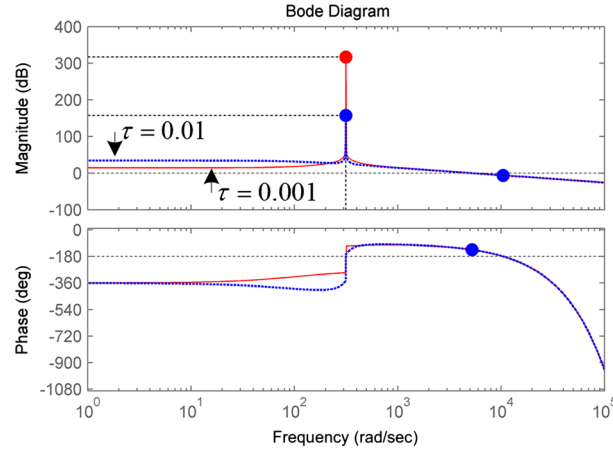


Figure 8. Bode diagram of the proposed PR controller.

$$i_{gdq}^{*-} = i_{odq}^{-} \quad (44)$$

where superscript ‘-’ denotes the negative sequence quantity. As $i_o = i_g - i_s$, considering the cost reduction of current sensors, (44) can be written as

$$i_{gdq}^{*-} = (i_g - i_s)_{dq}^{-} \quad (45)$$

However, as a part of the current reference, it is necessary to extract the negative sequence current components in (45).

Furthermore, as for the reference i_g^{+*} (superscript ‘+’ denotes the positive sequence quantity), the D -axis current component i_{gd}^{+*} can be obtained from the common DC-link voltage regulator, whereas the Q -axis current component i_{gq}^{+*} depends on the reactive power requirement, which has been beyond the scope of this paper. Here, let $i_{gq}^{+*} = 0$ for simplicity. However, the positive and negative sequence current reference quantities should be converted to the stationary reference frame first, then added with each other, i.e.

$$i_{g\alpha\beta}^* = i_{gdq}^{+*} e^{j\theta_u} + i_{gdq}^{-*} e^{-j\theta_u} = i_{g\alpha\beta}^{+*} + i_{g\alpha\beta}^{-*} \quad (46)$$

Hence, PR controllers can be used to obtain the required control effect.

To prevent the damages to the converters from over-current and over-voltage, for the SSC, the reference currents are revised as follows: if $\sqrt{(i_{g\alpha}^*)^2 + (i_{g\beta}^*)^2} > I_m$, then $i_{g\beta}^*$ is set to $i_{g\beta}^* = \sqrt{I_m^2 - (i_{g\alpha}^*)^2}$, where I_m is the maximum permitted current amplitude. Otherwise, they need not to be modified. The common DC-link voltage over-voltage protection is realized by using the brake resistor (similar to crowbar). When the DC-link voltage is larger than a specific value, the brake resistor starts to work until the DC-link voltage drops to a safe position. In fact, the brake resistor can be used to dissipate the redundant energy in such a generation system.

4. SIMULATION

In order to verify the effectiveness of the proposed control scheme under balanced and unbalanced loads, some numerical simulations using MATLAB/Simulink software have been carried out on the stand-alone wind power system based on DFIG.

In the simulations, the basic simulated configuration is shown in Figure 1, and the parameters of the DFIG are listed in Table I. The electrolytic capacitor C across the common DC-link is selected as 1000 μ F, and the DC-link reference voltage is set to 600 V. Besides, the values of the inductor and capacitor are 5 mH and 15 μ F, respectively. The reference stator line-to-line voltage of DFIG is 380 V/50 Hz.

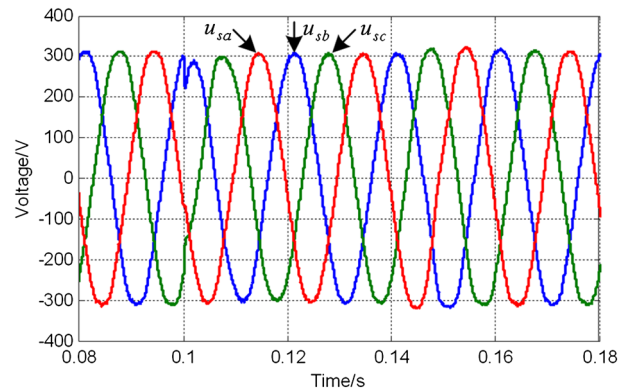
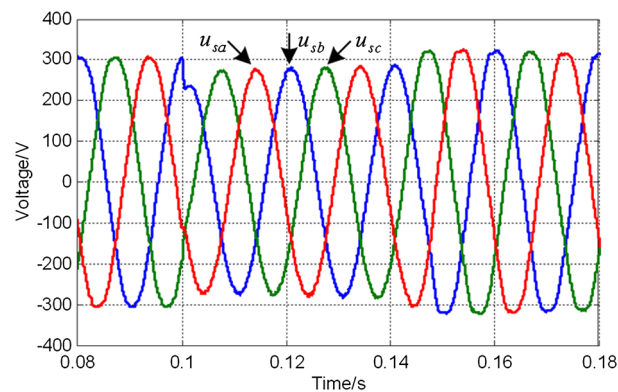
Table I. Parameters of the simulated DFIG.

Rated Power	3.7 kW
Stator voltage/frequency	220 V/50 Hz
Pole pairs	4
R_s	1.115 Ω
R_r	1.083 Ω
L_s	0.2096 H
L_r	0.2096 H
L_m	0.2037 H

4.1. Balanced loads

Under the stand-alone balanced load condition, the dynamic behaviors with load and generator speed variation are simulated on the wind power system based on DFIG. Figures 9 and 10 show the simulation results of the stator voltage under ADRC and PI control in the case of load variation. Before $t=0.1$ s, only the three-phase balanced series RL loads ($R=40\ \Omega$ and $L=5$ mH) are connected to the stator terminal; during the interval $t=0.1\sim 0.14$ s, another three-phase balanced paralleled resistive loads ($R=30\ \Omega$) are switched to the stator terminal; then, after $t=0.14$ s, the paralleled resistive loads are removed. From Figure 9, both the steady-state tracking performance and dynamic response of the stator voltage behave very well under the ADRC strategy. The stator voltages can return to its steady state quickly with the step change load. The simulation result of the stator voltages under conventional PI control with the same load variations is shown in Figure 10. By contrast, its dynamic response is relatively slow and there exists obvious dynamic error during transients.

To test the response to external mechanical disturbance, assume that the generator speed varies according to the profile shown as Figure 11. Before $t=0.1$ s, the generator speed is set to 620 rpm (sub-synchronous mode), and during the interval $t=0.1\sim 0.2$ s, the speed changes to synchronous speed 750 rpm; then, after $t=0.2$ s, the generator starts to operate at the speed

**Figure 9.** Simulation result of the stator voltages under ADRC in the case of load variation.**Figure 10.** Simulation result of the stator voltages under PI control in the case of load variation.

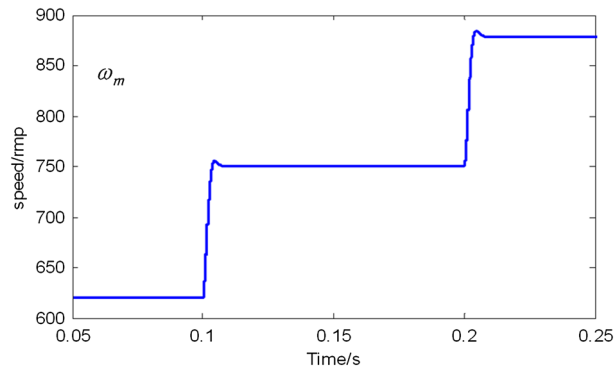


Figure 11. Speed profile of the generator.

of 880 rpm (super-synchronous mode). Figure 12 shows the stator voltage waveforms during a speed change of generator under ADRC, and it can be seen that there exists almost negligible voltage variation. The corresponding rotor current waveforms are illustrated in Figure 13. The simulation results show that as the DFIG operates at the synchronous speed during $t=0.1 \sim 0.2$ s, the rotor currents are almost DC currents. Meanwhile, the rotor currents have opposite phase sequence before $t=0.1$ s and after $t=0.2$ s, which corresponds to the natural properties of sub-synchronous and super-synchronous modes. Figures 14 and 15 show the simulation results of the stator voltages and rotor currents under PI control. As can be seen, the rotor current waveforms exhibit relatively smooth at the cost of inner current-loop control.

By comparisons between the two different control methods, it can be found that the control performance of ADRC is superior to that of PI control in the case of load disturbance, but there are no obvious performance differences with respect to the speed variation of generator. In addition, there are some oscillations in the rotor currents under ADRC, due to the lack of direct rotor current feedback.

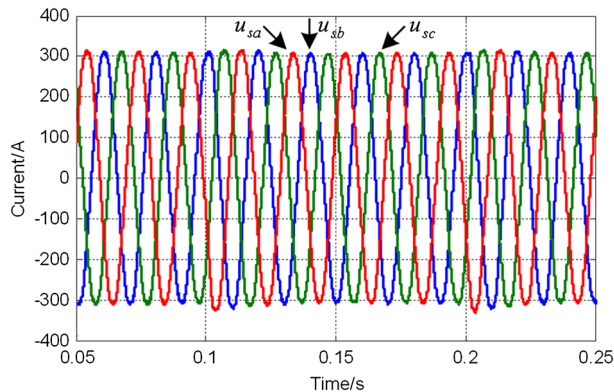


Figure 12. Simulation result of the stator voltages under ADRC in the case of speed variation of generator.

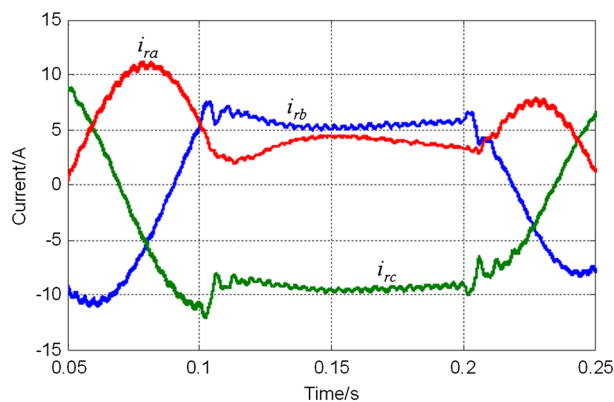


Figure 13. Simulation result of the rotor currents under ADRC in the case of speed variation of generator.

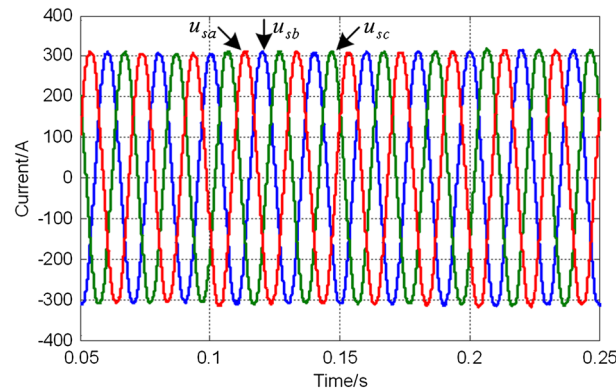


Figure 14. Simulation result of the stator voltages under PI control in the case of speed variation of generator.

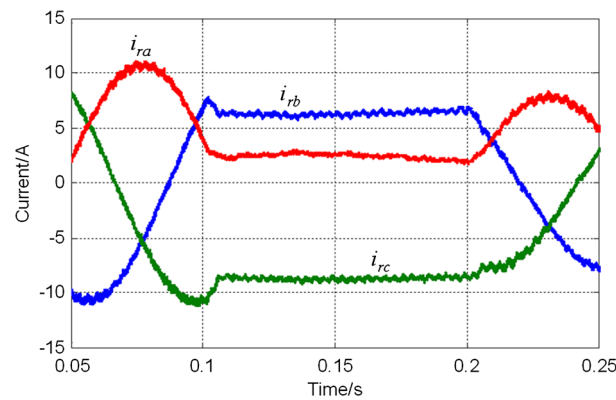


Figure 15. Simulation result of the rotor currents under PI control in the case of speed variation of generator.

4.2. Unbalanced loads

Under unbalanced load conditions, to verify the effectiveness of the coordinated control scheme of the SSC and RSC, some simulations are carried out with and without compensating the negative sequence load currents. Here, before $t=0.15$ s, the three-phase balanced series RL load ($R=40\ \Omega$ and $L=5$ mH) are connected to the stator terminal; during the interval $t=0.15\sim 0.25$ s, a per-phase paralleled resistive load ($R=20\ \Omega$) is switched to A-phase, which forms the unbalanced loads; after $t=0.25$ s, the per-phase paralleled resistive load is removed. In this section, the improved PR control methods proposed in the previous section are used.

The simulation results without compensating the negative sequence load currents are shown in Figures 16–20, where the stator voltages, stator currents, electromagnetic torque, common DC-link voltage and AC-side currents of the SSC are illustrated, respectively. From Figures 6–18, during the unbalanced load interval, serious stator voltage distortion occurs, the stator

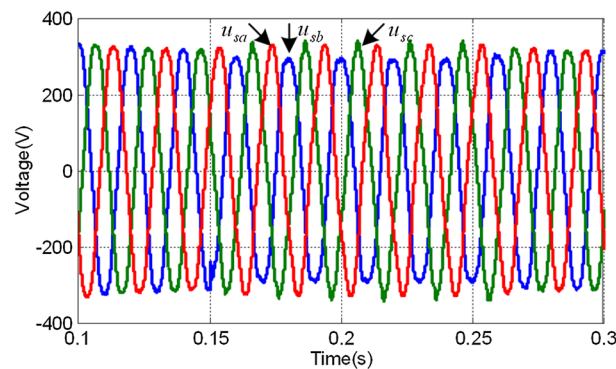


Figure 16. Simulation result of the stator voltages without compensation in the case of unbalanced load.

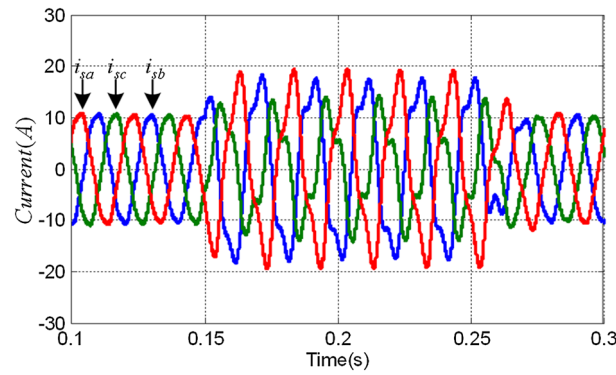


Figure 17. Simulation result of the stator currents without compensation in the case of unbalanced load.

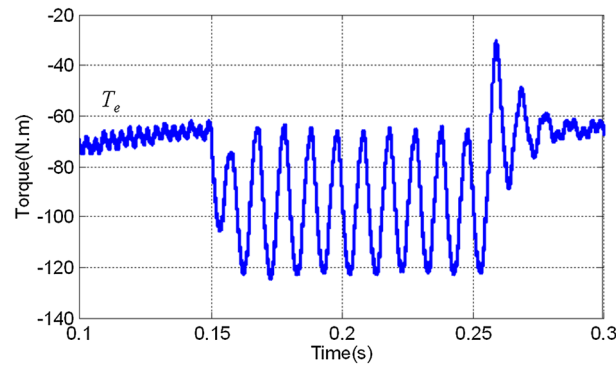


Figure 18. Simulation result of the electromagnetic torque of DFIG without compensation in the case of unbalanced load.

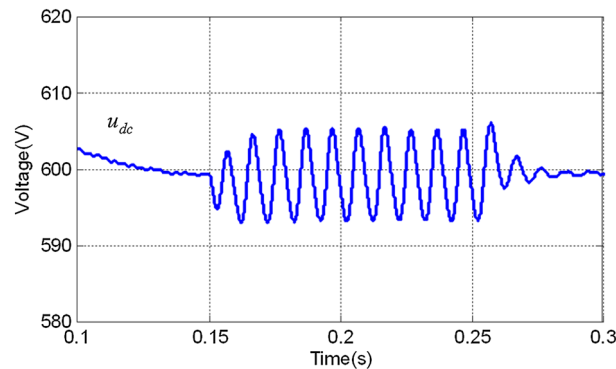


Figure 19. Simulation result of the common DC-link voltage without compensation in the case of unbalanced load.

currents are disturbed by the negative sequence components, and the electromagnetic torque pulsations increase, which will do harm to the DFIG. Besides, some oscillations appear in the common DC-link voltage shown in Figure 19. Figure 20 shows that the AC-side currents of SSC exhibit irregular fluctuations introduced by the negative sequence components.

When the negative sequence compensation method is applied, the corresponding simulation results are shown in Figures 21–25, where the stator voltages, stator currents, electromagnetic torque, common DC-link voltage and AC-side currents of the SSC are also illustrated, respectively. From Figures 21–24, by comparison with the uncompensated situations, there is no obvious voltage distortion but a slight voltage dip in the stator voltages even during the unbalanced load interval, due to the negative sequence compensation. The stator currents are improved and the electromagnetic torque pulsations are reduced greatly, which also proves the accuracy of the proposed control scheme. The oscillation of the common DC-link voltage is induced by the AC power delivery between loads and common DC-link capacitor. The AC-side current waveforms of the SSC show severe unbalance during the unbalanced load interval, because they take the responsibility for the negative sequence compensation of load currents.

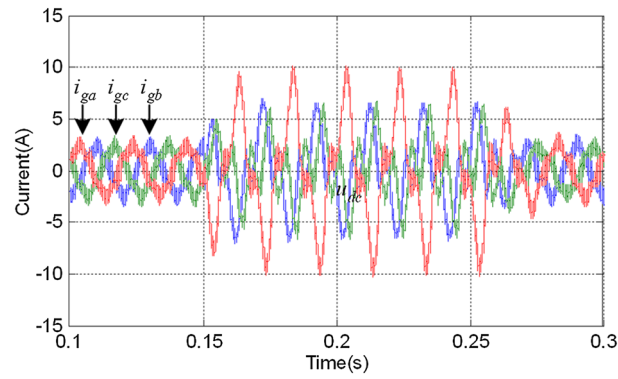


Figure 20. Simulation result of the AC-side currents of the SSC without compensation in the case of unbalanced load.

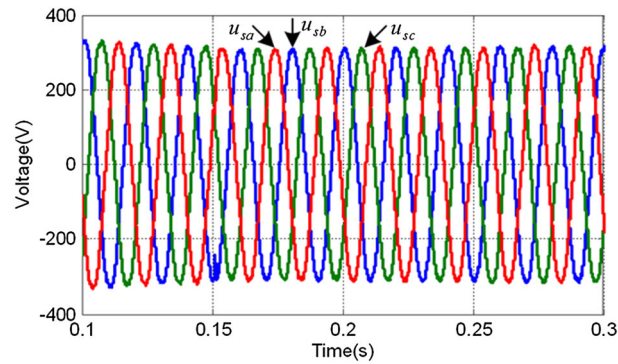


Figure 21. Simulation result of the stator voltages with compensation in the case of unbalanced load.

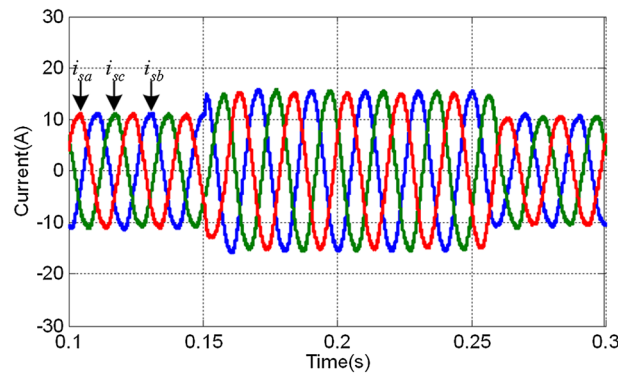


Figure 22. Simulation result of the stator currents with compensation in the case of unbalanced load.

With the aid of coordinated control, the SSC and RSC, the torque pulsation has been reduced greatly, and the balanced stator voltage could be guaranteed successfully. Figure 26 shows the overall simulation result of the stator voltage with the coordinated control.

5. EXPERIMENT

The experimental setup of a stand-alone DFIG system rated at 3.7 kW, as shown in Figure 27, composes of a DFIG, a back-to-back converter, loads and a control board based on DSP TMS320LF2812. The DFIG is driven by an induction motor (prime mover) controlled in speed mode, and its parameters are the same as those in the simulations earlier. For simplicity, the three-phase unbalanced loads with $R_a = 75 \, \Omega$ and $R_b = R_c = 25 \, \Omega$ that match the prime mover well are used in this experiment.

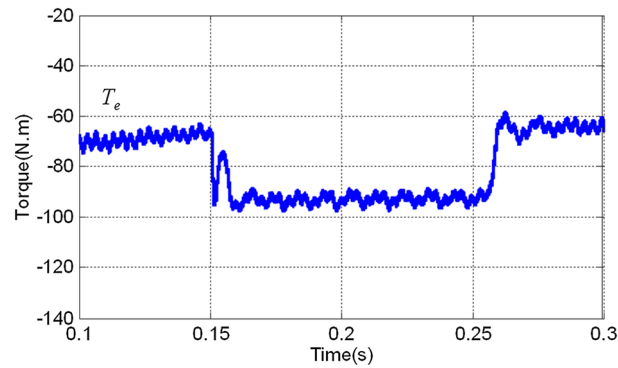


Figure 23. Simulation result of the electromagnetic torque of DFIG with compensation in the case of unbalanced load.

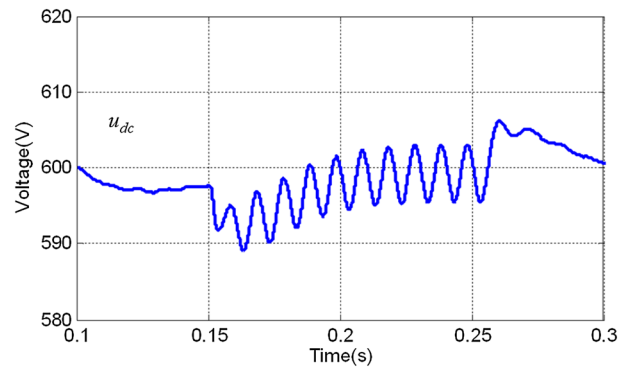


Figure 24. Simulation result of the common DC-link voltage with compensation in the case of unbalanced load.

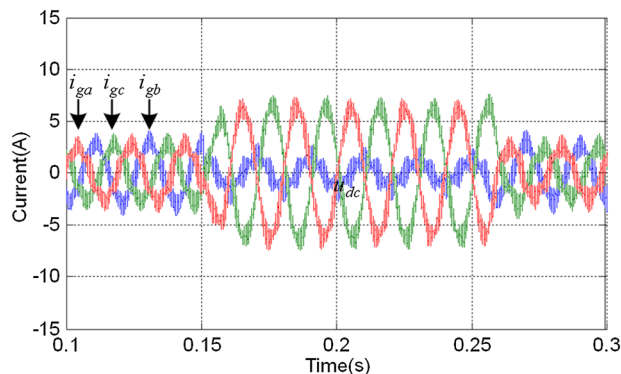


Figure 25. Simulation result of the AC-side currents of the SSC with compensation in the case of unbalanced load.

At first, the steady-state performance with respect to output voltage is tested under the unbalanced load condition. Figure 28 shows the experimental results of the output voltages in that case (at the rotor speed of 600 rpm), which have been balanced with the proposed control scheme. Besides, the corresponding load currents, DC-link voltage and absorbed currents by the SSC are shown in Figures 29 and 30, respectively.

To test the dynamic performance of the DFIG system with respect to load disturbance, R_a is changed from 75 to 25 Ω suddenly during the steady-state operation under unbalanced load condition, which means that the three-phase loads recover to be balanced. The transient response of the output voltages and load currents are depicted in Figure 31. It can be found that the output voltages only have a little fluctuation, which proves that the proposed control method behaves well in terms of the dynamic performance. Moreover, when the rotor speed is changed from super-synchronous mode (760 rpm) to sub-synchronous mode (720 rpm), the corresponding output stator voltage and rotor current are shown in Figure 32. As seen, it can be concluded that the output voltage is robust to the speed variation of prime mover.

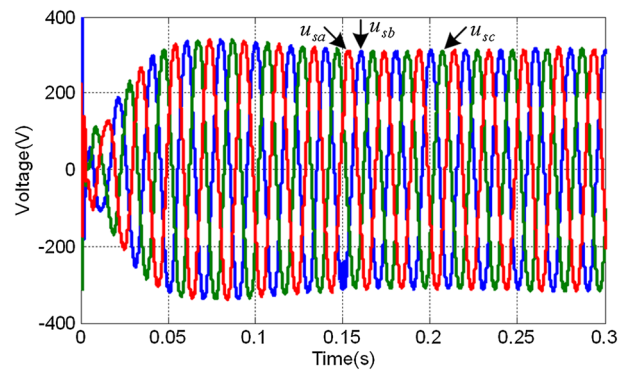


Figure 26. Simulation result of the overall stator voltages.

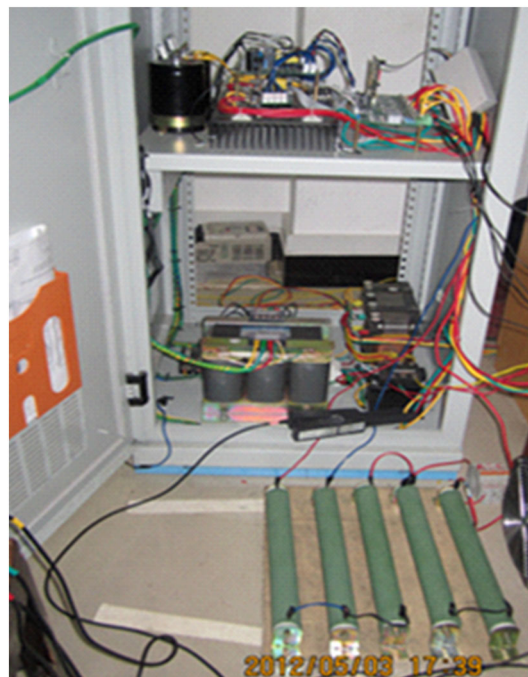


Figure 27. Prototype of a 3.7 kW DFIG control system.

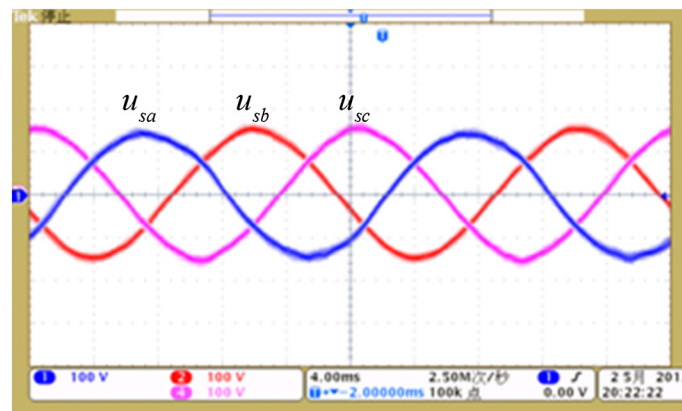


Figure 28. The steady-state output voltages under the unbalanced load condition.

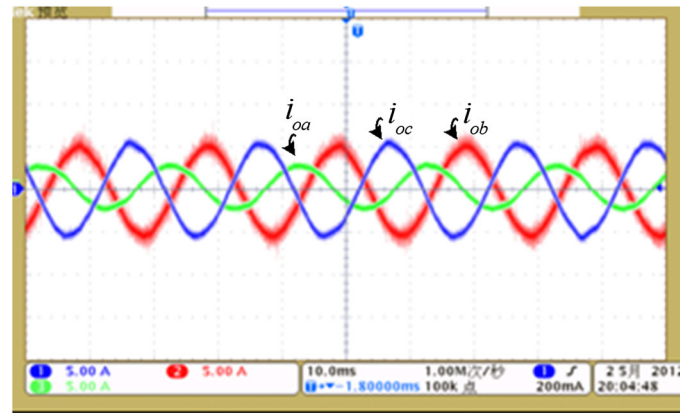


Figure 29. Load current waveforms under the unbalanced load condition.

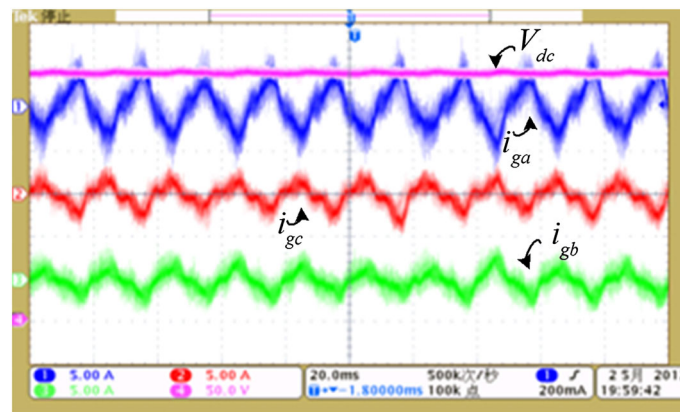


Figure 30. DC-link voltage and AC-side currents of the SSC under the unbalanced load condition.

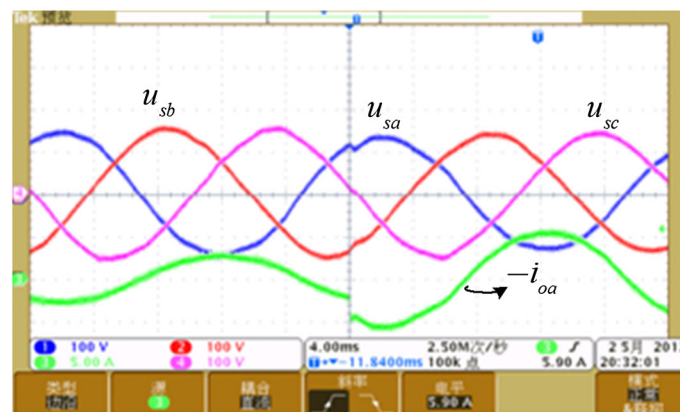


Figure 31. Output voltages and A-phase load current under the load variation.

6. CONCLUSIONS

In this paper, a new coordinated control scheme for the SSC and RSC to compensate for the unbalanced load of the stand-alone wind energy conversion system based on DFIG has been proposed. Since ADRC is used to control the stator voltage achieved by the RSC, the system dynamic response and steady-state performance has been improved because of the nonlinear high gain ESO and SFC. In addition, there is no need of current sensor for rotor; so, it is a cost effective method. For the control of the

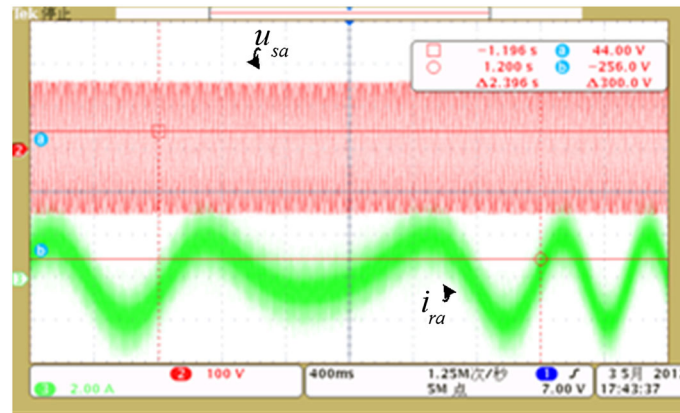


Figure 32. A-phase stator voltage and rotor current under rotor speed variation.

SSC, an improved PR control design method is presented in this paper, which can provide more degrees of freedom in the trade-off between the dynamic response and steady-state performance and also simplify the system control under unbalanced load condition. With the negative sequence currents compensated by the SSC, the oscillations in the machine can be eliminated, and the performance of the stand-alone wind energy conversion system is improved greatly. The simulation and experimental results verify the effectiveness and correctness of the proposed coordinated control scheme.

ACKNOWLEDGEMENT

This work is supported by the National High Technology Research and Development Program of China (SS2012AA051601).

REFERENCES

1. Pena R, Clare JC, Asher GM. Double fed induction generator using back-to-back PWM converter and its application to variable-speed wind energy generation. *IEE Proceedings on Electric Power Applications* 1996; **143**(3): 231–241.
2. Muller S, Deicke M, Doncker RWD. Doubly fed induction generator systems for wind turbines. *IEEE Industry Applications Magazine* 2002; **8**(3): 26–33.
3. Shen B, Mwinyiwiwa B, Zhang YZ, Ooi BT. Sensor-less maximum power point tracking of wind by DFIG using rotor position phase lock loop (PLL). *IEEE Transactions on Power Electronics* 2009; **24**(4): 942–951.
4. Smith AC, Todd R, Barnes M, Tavner PJ. Improved energy conversion for doubly fed wind generators. *IEEE Transactions on Industry Applications* 2006; **42**(6): 1421–1428.
5. Chen SZ, Cheung NC, Wong KC, Wu J. Integral sliding-mode direct torque control of doubly-fed induction generators under unbalanced grid voltage. *IEEE Transactions on Energy Conversion* 2010; **25**(2): 356–368.
6. Xu L, Cartwright P. Direct active and reactive power control of DFIG for wind energy generation. *IEEE Transactions on Energy Conversion* 2006; **21**(3): 750–758.
7. Iwanski G, Koczara W. DFIG-based power generation system with UPS function for variable-speed applications. *IEEE Transactions on Industrial Electronics* 2008; **55**(8): 3047–3054.
8. Pena R, Asher GM, Clare JC. A doubly fed induction generator using back to back PWM converters supplying an isolated load from a variable speed wind turbine. *Proc. Inst. Elect. Eng., Electric Power Applications* 1996; **143**(5): 380–387.
9. Cardenas R, Pena R, Probst J, Asher G, Clare J. MRAS observer for sensorless control of standalone doubly fed induction generators. *IEEE Transactions on Energy Conversion* 2005; **20**(4): 710–718.
10. Iwanski G, Koczara W. Sensor-less direct voltage control of the stand-alone slip-ring induction generator. *IEEE Transactions on Industrial Electronics* 2007; **54**(2): 1237–1239.
11. Bansal RC. Three-phase self-excited induction generators: an overview. *IEEE Transactions on Energy Conversion* 2005; **20**(2): 292–299.
12. Xu L. Coordinated control of DFIG's rotor and grid side converters during network unbalance. *IEEE Transactions on Power electronics* 2008; **23**(3): 1041–1049.

13. Hu JB, He YK. Reinforced control and operation of DFIG-based wind-power-generation system under unbalanced grid voltage conditions. *IEEE Transactions on Energy Conversion* 2009; **24**(4): 905–915.
14. Phan VT, Kwak SH, Lee HH. An improved control method for DFIG-based wind system supplying unbalanced stand-alone loads. *ISIE 2009* 2009; 1081–1086.
15. Jain AK, Ranganathan VT. Wound rotor induction generator with sensor-less control and integrated active filter for feeding nonlinear loads in a stand-alone grid. *IEEE Transactions on Industrial Electronics* 2008; **55**(1): 218–228.
16. Pena R, Cardenas R, Escobar R, Clare E, Wheeler P. Control system for unbalanced operation of stand-alone doubly-fed induction generators. *IEEE Transactions on Energy Conversion* 2007; **22**(2): 544–545.
17. Han J. From PID to active disturbance rejection control. *IEEE Transactions on Industrial Electronics* 2009; **56**(3): 900–906.
18. Yepes G, Freijedo FD, Doval-Gandoy J, Lopez O, Malvar J, Fernandez-Comesana P. Effects of discretization methods on the performance of resonant controllers. *IEEE Transactions on Power Electronics* 2010; **25**(7): 1692–1712.
19. Yuan X, Merk W, Stemmler H, Allmeling J. Stationary-frame generalized integrators for current control of active power filters with zero steady-state error for current harmonics of concern under unbalanced and distorted operating conditions. *IEEE Transactions on Industry Applications* 2002; **38**(2): 523–532.